ACCSCIENCE PUBLISHING

Eurasian Journal of Medicine and Oncology

ORIGINAL RESEARCH ARTICLE

Exploring the therapeutic potential of gamma-glutamyl carboxylase in prostate cancer through integrated multi-omics analysis

Yuangao Xu[1†], Jieyu Xiong[2†], Yuanbo Xu[3], YiKun Wu[4], Yuanlin Wang[5], Hua Shi[5*], and Shuxiong Xu[5*]

[1]Department of Organ Transplantation, Guizhou Provincial People's Hospital, Guiyang, Guizhou, China

[2]Department of Biomedical Research, Faculty of Medicine, University of Bern, Bern, Switzerland

[3]Department of Clinical Medicine, School of Medicine, Southern Medical University, Guangzhou, Guangdong, China

[4]Department of Clinical Medicine, School of Medicine, Guizhou University, Guiyang, Guizhou, China

[5]Department of Urology, Guizhou Provincial People's Hospital, Guiyang, Guizhou, China

Abstract

Introduction: Prostate cancer (PCa) treatment is often limited by heterogeneous therapeutic responses and the emergence of drug resistance, underscoring the urgent need to identify novel therapeutic targets.

Objective: This study aims to identify novel susceptibility genes associated with PCa risk by integrating genomic, transcriptomic, and proteomic data.

Methods: We performed a genome-wide summary-data-based Mendelian randomization (SMR) analysis leveraging cis-expression quantitative trait loci from multiple tissues and PCa phenotypes. We then applied Bayesian colocalization to confirm that the observed SMR signals reflected shared causal variants. To characterize gamma-glutamyl carboxylase (GGCX) expression in normal and malignant prostate tissues, we integrated bulk transcriptomic and proteomic data from The Cancer Genome Atlas, Gene Expression Omnibus, the International Cancer Genome Consortium, and the Human Protein Atlas. We further investigated the spatial distribution of GGCX within the tumor microenvironment using spatial transcriptomics and Spearman correlation analyses with key stromal and immune cell markers. Finally, we constructed a GGCX-centered gene set by combining weighted gene co-expression network analysis with a random forest model and performed GO and KEGG enrichment analyses to infer its potential biological functions and pathways.

Results: SMR identified 53 candidate genes associated with PCa phenotypes, including GGCX ($p<0.001$), and confirmed the association of GGCX using Bayesian colocalization (PP.H4 > 0.95). GGCX expression was higher in PCa tissues than in normal prostate tissues ($p<0.001$), and it was positively correlated with tumor cell abundance but inversely correlated with fibroblast content in PCa. We further found that a GGCX-associated gene set was enriched in the ubiquinone and terpenoid-quinone biosynthesis pathway, particularly the vitamin K cycle.

Conclusion: Our multi-omics data highlight the GGCX–vitamin K axis as a genetically supported and druggable pathway in PCa.

Keywords: Susceptibility gene; Gamma-glutamyl carboxylase; Prostate cancer; Multi-omics study

†These authors contributed equally to this work.

***Corresponding authors:**
Hua Shi
(shihua@gz5055.com);
Shuxiong Xu
(xushuxiong@gz5055.com)

Citation: Xu Y, Xiong J, Xu Y, *et al.* Exploring the therapeutic potential of gamma-glutamyl carboxylase in prostate cancer through integrated multi-omics analysis. *Eurasian J Med Oncol*. 2026;10(5):025320342. doi: 10.36922/EJMO025320342

Received: August 4, 2025

Revised: December 1, 2025

Accepted: December 10, 2025

Published online: January 22, 2026

Copyright: © 2026 Author(s). This is an Open Access article distributed under the terms of the Creative Commons Attribution License, permitting distribution, and reproduction in any medium, provided the original work is properly cited.

Publisher's Note: AccScience Publishing remains neutral with regard to jurisdictional claims in published maps and institutional affiliations.

1. Introduction

Prostate cancer (PCa) remains one of the most prevalent malignancies among men globally, with notable variations in incidence and mortality rates across different regions and populations.[1] Epidemiological studies have consistently shown that while developed countries report higher incidence rates of PCa, mortality rates remain relatively low, primarily due to early screening practices and effective therapeutic interventions.[1,2] PCa typically presents with symptoms, such as increased urinary frequency, urgency, weak urinary flow, and painful urination, significantly impacting patients' quality of life.[3] Current treatment modalities include surgical resection, radiotherapy, hormone therapy, and chemotherapy.[4] Although these treatments have extended patient survival, their efficacy varies among individuals, and challenges, such as recurrence and drug resistance persist.[3]

Recent studies have revealed that approximately 30% of patients eventually progress to castration-resistant PCa, a form of disease that responds poorly to most conventional treatments.[5] This progression is driven by intricate molecular reprogramming, where tumor cells exhibit significant metabolic plasticity, such as the shift toward oxidative phosphorylation, and activate adaptive survival mechanisms to evade therapy.[6,7] Concurrently, cancer cells employ diverse escape mechanisms, including altered mitochondrial function, dysregulated autophagy pathways, and the acquisition of invasive and metastatic phenotypes, further limiting therapeutic durability.[8,9] Importantly, this molecular complexity is exacerbated by substantial genomic, transcriptomic, and proteomic variability both within and between tumors, leading to heterogeneous clinical outcomes and variable treatment responses.[10,11] Such inter-patient and intra-tumoral heterogeneity underscores a critical gap: The lack of precision biomarkers and actionable molecular targets that can guide individualized therapeutic decision-making. Therefore, identifying novel susceptibility genes and dissecting the specific molecular pathways underlying PCa initiation, progression, and resistance have emerged as essential strategies for developing more precise, mechanism-based targeted interventions.

This study aims to identify novel susceptibility genes associated with PCa risk by integrating genomic, transcriptomic, and proteomic data. By employing a comprehensive multi-omics approach, we investigated the expression patterns and potential functions of candidate genes across various tissue types and cell populations within the PCa microenvironment. Our findings could potentially uncover new therapeutic targets and improve treatment outcomes for PCa patients.

2. Materials and methods

2.1. Summary-data-based Mendelian randomization (SMR) analysis

We integrated cis-expression quantitative trait loci (eQTL) summary statistics from the Genotype-Tissue Expression (GTEx; https://gtexportal.org/home/) whole blood dataset,[12] a medium-sized multi-tissue RNA sequencing resource, with those from the large-scale, blood-specific eQTLGen meta-analysis to capture complementary aspects of blood-derived genetic regulation of gene expression.[13] PCa cases were defined in FinnGen (R12) using *International Classification of Diseases for Oncology*, Third Edition, codes[14] and in the UK Biobank using PheCode mappings of *International Statistical Classification of Diseases and Related Health Problems 10th Revision* diagnoses,[15] restricting analyses to pathologically confirmed prostate adenocarcinoma where possible (Table S1). We considered only cis-eQTLs located within 1 Mb of the gene body, with genome-wide significant association with blood-based expression ($p<5 \times 10^{-8}$) and minor allele frequency >1%.[16] The Heterogeneity in Dependent Instruments test was applied to each SMR association to distinguish pleiotropy from linkage; $p>0.05$ was taken to indicate no evidence of heterogeneity in single-nucleotide polymorphism (SNP) effects on expression and PCa, and thus a valid instrument for SMR.[17]

2.2. Bayesian colocalization analysis

We performed Bayesian colocalization to evaluate whether eQTL and PCa association signals at each locus were driven by shared or distinct causal variants.[18] We computed posterior probabilities for five hypotheses:

(i) PP.H0: No causal variants in either eQTLs or PCa within the locus.
(ii) PP.H1: A causal variant only in the eQTLs.
(iii) PP.H2: A causal variant only in PCa.
(iv) PP.H3: Distinct causal variants in both eQTLs and PCa.
(v) PP.H4: A shared causal variant influences both eQTLs and PCa.

Colocalization windows were defined as ±1 Mb around each eQTL.[19] We considered PP.H4 of 0.75 as evidence of colocalization, in line with previous work.[20]

2.3. Differential gene expression analysis

Paired transcripts per million expression data from normal samples in the GTEx database and tumor samples in The Cancer Genome Atlas (TCGA) database were retrieved from the UCSC Xena platform.[21] Expression values were standardized to unitless Z-scores to ensure data comparability using Equation (1) for each tumor group:

$$Z = \frac{x - \mu}{ó} \quad (1)$$

Z-score standardization facilitated the identification and removal of outliers, where values exceeding ±3.0 were excluded to minimize their impact on analytical accuracy. Receiver Operating Characteristic (ROC) analysis was performed using the pROC package to evaluate the diagnostic performance of gene expression in distinguishing tumors from normal groups. Validation was carried out using datasets extracted from Gene Expression Omnibus (GEO; Table S1). The statistical differences in gene expression between tumor and normal tissues were assessed using the Wilcoxon rank-sum test.

2.4. Spatial transcriptomics analysis

Spatial transcriptomics analyses were performed using the Spatial Tumor Microenvironment (SpatialTME) database, which provides curated spatial transcriptomic profiles of PCa together with matched single-cell RNA sequencing-derived reference signatures for major tumor, stromal, and immune cell types.[22] For each sample, we applied quality control at the spot level, excluding spots with excessively low or excessively high numbers of detected genes, extreme Unique Molecular Identifier counts, or elevated mitochondrial RNA fractions, to minimize technical noise and low-quality capture.[23]

To infer cell-type composition within each spatial spot, we first constructed a signature matrix by calculating the mean expression of the top 25 marker genes for each annotated cell type in the reference single-cell dataset. Using this matrix, we computed cell-type enrichment scores for all spots with the Cottrazm package, and visualized the spatial distribution of individual cell types and of gamma-glutamyl carboxylase (GGCX) expression with the SpatialFeaturePlot function in Seurat, where higher color intensity reflects higher inferred abundance or expression.[24] Tumor core spots were defined by clustering morphology-adjusted expression matrices and identifying clusters with high inferred copy-number variation burden, consistent with malignant epithelial compartments; adjacent "border" spots were then assigned based on their proximity in the UMAP embedding to the centroid of the tumor core cluster, and more distant spots were classified as normal-like. Differential gene expression between spatially defined regions (tumor core, border, and normal-like) was assessed using the Wilcoxon rank-sum test implemented in R (wilcox.test), and results were summarized as bar plots to compare relative expression levels across groups. Similar deconvolution-based spatial approaches have been widely adopted to characterize tumor, stromal, and immune cell distributions within the tumor microenvironment in solid cancers.[25]

2.5. Gene enrichment analysis and clustering

Tumor samples from the TCGA database were categorized into two groups according to GGCX expression, using a threshold of 0.3 on the normalized expression values. Differential expression analysis was performed with the limma package, identifying significant genes with $|\log FC| > 0.585$ and adjusted $p<0.05$. Single-cell expression profiles were retrieved from the Tumor Immune Single-Cell Hub 2 (TISCH2) database to assist in annotating cell-type–specific expression patterns.[26] Before weighted gene co-expression network analysis (WGCNA),[27] data were quality-controlled and normalized. Hierarchical clustering of gene expression in PCa was conducted using the pheatmap and WGCNA packages, optimized with Euclidean distance and Ward's variance method (ward.D2). Functional enrichment analyses, including Gene Ontology (GO)[28] and Kyoto Encyclopedia of Genes and Genomes (KEGG),[29] were conducted using clusterProfiler[30] and pathview.[31] To validate these findings, KEGG metabolic pathway scores from the International Cancer Genome Consortium (ICGC)[32] were calculated with the Gene Set Variation Analysis (GSVA) package (z-score method), and high- and low-expression groups were defined as the top and bottom 30% of samples. Differences in pathway scores were evaluated using the limma package.

2.6. Statistical analysis

All analyses were performed in R (v4.3.3), using dedicated packages, including coloc (v5.1.1) and SMR (v1.03) for genetic analyses, and limma, pROC, Seurat, and GSVA for expression and pathway analyses. Unless otherwise specified, statistical tests were two-sided. For high-dimensional analyses, p-values were adjusted using the Benjamini–Hochberg false discovery rate (FDR) procedure, with FDR <0.05 considered statistically significant, whereas a nominal $p<0.05$ was applied for descriptive or exploratory comparisons.

3. Results

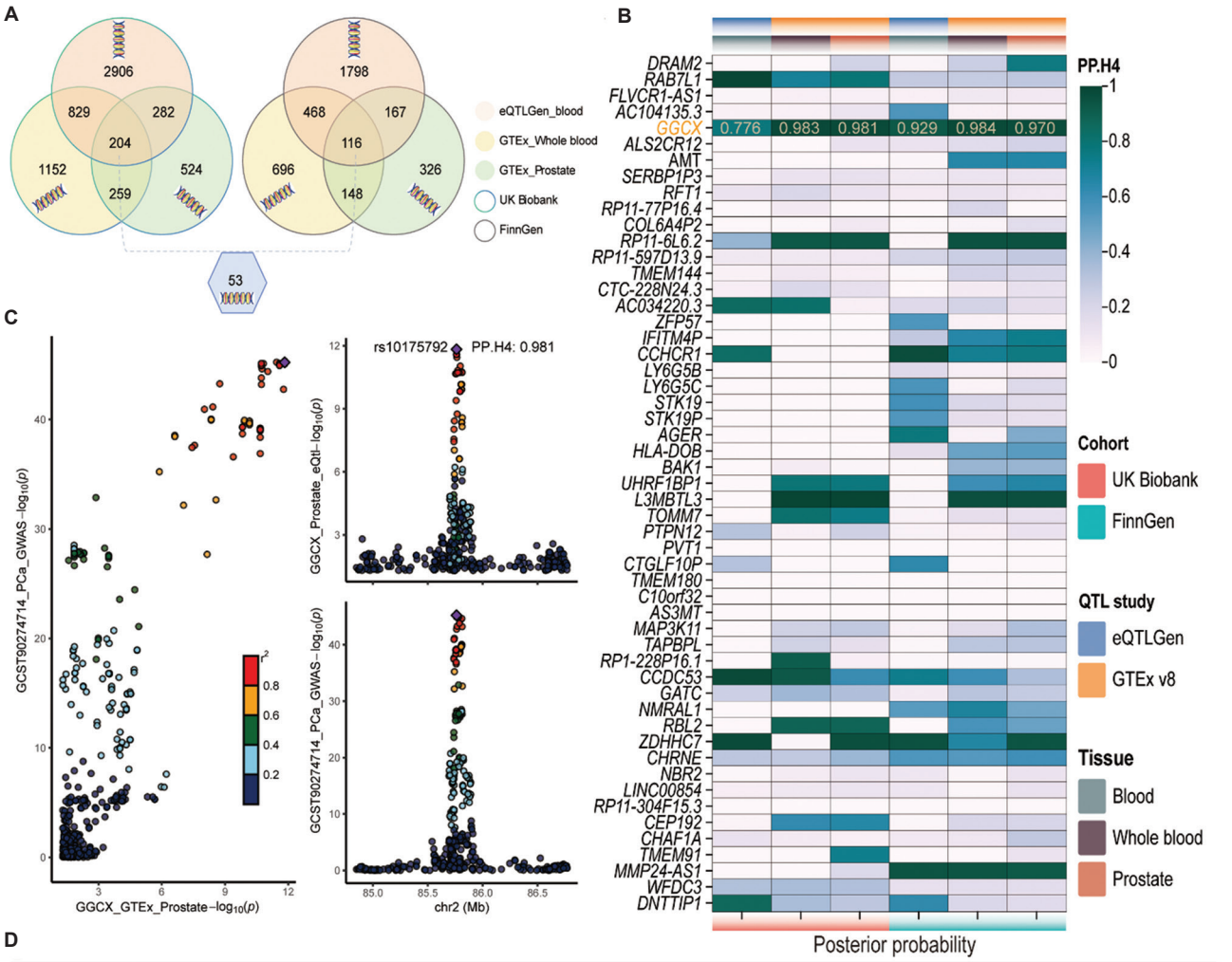
3.1. Identification of 53 susceptibility genes via genome-wide SMR

Germline variants predisposing to PCa are thought to act largely by modulating gene expression in disease-relevant tissues, particularly the prostate itself and immune- or inflammation-related compartments that can be captured in blood-derived expression datasets.[33] On this basis, we focused our SMR analyses on eQTLs derived from blood and prostate tissues together with summary statistics for phenotypic PCa. After applying rigorous filters of SMR_$p<0.05$, 2,906 genes were identified in the blood group (Figure 1A), 1,152 genes in the whole blood group (Figure 1B), and 524 genes in the prostate



Figure 1. Volcano plots illustrate the association between susceptibility genes and prostate cancer risk. The x-axis represents the odds ratio (OR) effect size, and the y-axis indicates the –log10 (*p*-value). Results are derived from the UK Biobank cohort (A-C) and the FinnGen cohort (D-F), and are presented for gene expression data from three tissue sources: blood (A and D), whole blood (B and E), and prostate (C and F) samples.

group (Figure 1C). The further intersection of the three groups of genes yielded 204 overlapping genes retained for downstream analysis. As a validation cohort, we repeated the analysis using the same eQTL sources but with phenotypic PCa data from FinnGen. Among them, 1,798 genes were identified in the blood group (Figure 1D), 696 genes in the whole blood group (Figure 1E), and 326 genes in the prostate group (Figure 1F). The further intersection of the three groups of genes resulted in 116 genes being included within the reference range. After intersecting the gene sets, 53 genes remained (Table S2) and were treated as candidate susceptibility genes (Figure 2A).



Gene	QTL study	Tissue	Trait	Cohort	Top SNP	Se	OR (95% CI)	SMR_p	HEIDI_p	SMR_p_FDR
GGCX	eQTLGen	Blood	PCa	UK Biobnak	rs35215812	0.019	0.783 (0.754 – 0.814)	2.18e−36	2.22e−08	5.53e−33
GGCX	GTEx v8	Blood	PCa	UK Biobnak	rs6738645	0.017	0.835 (0.808 – 0.863)	1.89e−26	9.96e−03	5.75e−23
GGCX	GTEx v8	Prostate	PCa	UK Biobnak	rs6743030	0.025	0.854 (0.813 – 0.897)	2.40e−10	5.90e−02	1.30e−07
GGCX	eQTLGen	Blood	PCa	FinnGen	rs35215812	0.040	0.833 (0.771 – 0.901)	4.27e−06	7.70e−02	1.37e−03
GGCX	GTEx v8	Blood	PCa	FinnGen	rs6738645	0.029	0.867 (0.819 – 0.917)	6.18e−07	8.83e−01	5.41e−04
GGCX	GTEx v8	Prostate	PCa	FinnGen	rs6743030	0.029	0.885 (0.836 – 0.938)	3.25e−05	7.14e−01	9.84e−03

Figure 2. Colocalization and summary-data-based Mendelian randomization (SMR) analyses of candidate genes and prostate cancer (PCa). (A) Flowchart illustrating the process for identifying susceptibility genes. (B) Heatmap depicting the posterior probability (PP.H4) from colocalization analyses between candidate susceptibility genes and PCa phenotype across different tissue types. The greener the color, the higher the PP.H4. (C) Scatter plots showing the colocalization analysis results for *GGCX* expression in prostate tissue and PCa. (D) Forest plot presenting the results of genome-wide SMR analysis for *GGCX* and PCa phenotype across multiple tissues.

Abbreviations: FDR: False discovery rate; HEIDI: Heterogeneity in Dependent Instruments; OR: Odds ratio; QTL: Quantitative trait loci; SNP: Single-nucleotide polymorphism.

3.2. Genetic colocalization analysis of candidate genes and PCa

We performed Bayesian colocalization analyses to assess whether the genetic signals for gene expression and PCa risk were driven by shared causal variants across tissues. In the UK Biobank cohort, we observed high posterior probabilities for a shared causal variant (PP.H4) for several genes, including *GGCX* (whole blood: 0.983, prostate: 0.981), *L3MBTL3* (whole blood and prostate: 0.999), *CCDC53* (blood: 0.985, whole blood: 0.931), *RBL2*

(whole blood: 0.985, prostate: 0.885), and *ZDHHC7* (blood: 0.979, prostate: 0.963). We also detected notable PP.H4 values for *RAB7L1*, *RP11-6L6.2*, *AC034220.3*, *CCHCR1*, *UHRF1BP1*, *TOMM7*, and *DNTTIP1* in different tissue types (Figure 2B).

In the FinnGen cohort, we again found strong evidence of colocalization for *GGCX* (blood: 0.929, whole blood: 0.984, prostate: 0.970), *RP11-6L6.2* (whole blood: 0.955, prostate: 0.956), *CCHCR1* (blood: 0.971), *L3MBTL3* (whole blood and prostate: 0.962), *ZDHHC7* (blood: 0.957, prostate: 0.946), and *MMP24-AS1* (blood: 0.946, whole blood: 0.944, prostate: 0.929), while *DRAM2* showed a notable PP.H4 in prostate tissue (0.758) (Figure 2B). When we considered consistency across both cohorts and all three tissue groups (blood, whole blood, and prostate), only *GGCX* showed robust colocalization with PCa (PP.H4 > 0.75 in all settings), suggesting that *GGCX* and PCa may share causal variants at the rs10175792 locus on chromosome 2 (85.5–86.0 Mb) in prostate tissue (Figure 2C). In line with these findings, we also noted that *GGCX* was significantly associated with PCa in the genome-wide SMR analysis (odds ratio [OR] < 1, SMR_p<0.05), and all p-values for *GGCX* passed FDR correction (SMR_p_FDR < 0.05), further strengthening the evidence that *GGCX* is a susceptibility gene for PCa (Figure 2D).

3.3. SMR analysis of GGCX from different tissue sources with phenotypic PCa

To determine whether *GGCX* expression in tissues beyond blood and prostate confers similar susceptibility to PCa, we next extended our SMR analyses across multiple GTEx tissues. We retrieved eQTL data for *GGCX* from adipose tissue, artery, brain, colon, heart, muscle, nerve, spleen, stomach, thyroid, skin, pancreas, esophagus, testis, fibroblasts, and vascular-derived lymphocytes, and tested genetically predicted *GGCX* expression in each tissue for association with PCa. In these cross-tissue analyses, the leading instrumental SNPs for *GGCX* included rs85788175, rs85764041, rs85769711, and rs85783128 (Figure 3). In the UK Biobank cohort, we found that *GGCX* expression derived from multiple tissues was significantly associated with PCa risk (OR < 1, SMR_p<0.05), suggesting a consistent protective direction of effect. We observed similar associations in the FinnGen cohort (Figure 3). Taken together, these cross-tissue and cross-cohort findings strengthen the evidence that genetically regulated *GGCX* expression is broadly associated with PCa susceptibility and may play a causal role in disease risk.

3.4. Expression of GGCX in tumor and normal tissues

We first examined GGCX protein expression in prostate tissues based on data from the Human Protein Atlas (HPA). We noted that the antibody HPA-018284 generated low-intensity signals predominantly in the cytoplasmic and membranous regions of glandular cells in both cancerous and normal prostate tissues (Figure 4A-D). To characterize GGCX expression at the cellular level within the tumor microenvironment, we next performed deconvolution analysis on spatial transcriptomics data to delineate tumor cells, border cells, and normal cells (Figure 4E). When we compared *GGCX* expression across these three cell populations, tumor regions showed significantly higher expression than border and normal regions (p<0.001, Figure 4F). We then integrated bulk transcriptomic data from TCGA and GTEx to evaluate *GGCX* expression in larger cohorts, and observed that *GGCX* levels were markedly higher in tumor samples than in normal prostate tissues (p<0.001, Figure 4G). We confirmed this differential overexpression in independent GEO datasets, where *GGCX* again showed consistently elevated expression in tumor tissues (Figure 4H and I). Finally, we assessed whether *GGCX* expression could aid in distinguishing PCa from normal prostate tissue. Using ROC analysis, we found that *GGCX* expression provided good diagnostic performance, with an area under the curve (AUC) of 0.783 (95% confidence interval [CI]: 0.750–0.816). The calibration curve further showed no significant deviation from the ideal model (p=0.992), indicating that the predicted probability based on *GGCX* expression closely matched the observed tumor status (Figure 4J and K).

3.5. Association between GGCX expression and immune infiltration in the prostate tumor microenvironment

We further visualized *GGCX* expression across spatial transcriptomic spots using the SpatialFeaturePlot function. In these maps, we observed *GGCX* expression in multiple cell populations, including B cells/plasma cells, macrophages, dendritic cells, endothelial cells, fibroblasts, and epithelial cells, but the signal co-localized most strongly with tumor cell-rich regions, suggesting that *GGCX* is predominantly expressed in tumor cells within the prostate tumor microenvironment (Figure 5A-L). To quantify these patterns, we then correlated *GGCX* expression with inferred cell-type abundances. We found that *GGCX* expression was negatively correlated with endothelial cells and fibroblasts, while positively correlated with tumor cells, neutrophils, dendritic cells, and plasma B cells, with the strongest correlation observed for tumor cells, in line with the spatial localization results (Figure 5M). Next, we sought to validate these enrichment patterns in independent datasets from the GEO database. Across these cohorts, we again observed that higher *GGCX* expression was primarily observed in tumor cells,

Gene	QTL study	Tissue	Trait	Cohort	Top SNP	Se	OR (95% CI)	SMR_p	HEIDI_p
GGCX	GTEx v8	Adipose	PCa	UK Biobnak	rs85788175	0.044	0.724 (0.664 – 0.789)	2.49e-13	2.68e-03
GGCX	GTEx v8	Artery	PCa	UK Biobnak	rs85762048	0.021	0.832 (0.799 – 0.866)	2.77e-19	2.35e-04
GGCX	GTEx v8	Brain	PCa	UK Biobnak	rs85764041	0.012	0.906 (0.885 – 0.927)	1.28e-16	4.03e-01
GGCX	GTEx v8	Blood vessel_fibroblasts	PCa	UK Biobnak	rs85758015	0.068	0.687 (0.601 – 0.785)	3.30e-08	2.67e-01
GGCX	GTEx v8	Blood vessel_lymphocytes	PCa	UK Biobnak	rs85783128	0.013	0.909 (0.887 – 0.932)	4.62e-14	1.57e-03
GGCX	GTEx v8	Colon	PCa	UK Biobnak	rs85764041	0.031	0.790 (0.743 – 0.840)	4.62e-14	3.71e-04
GGCX	GTEx v8	Heart	PCa	UK Biobnak	rs85796101	0.031	0.811 (0.763 – 0.861)	6.94e-12	9.12e-02
GGCX	GTEx v8	Muscle	PCa	UK Biobnak	rs85769711	0.028	0.799 (0.757 – 0.844)	6.66e-16	7.43e-03
GGCX	GTEx v8	Nerve	PCa	UK Biobnak	rs85788175	0.025	0.797 (0.759 – 0.837)	1.25e-19	9.23e-06
GGCX	GTEx v8	Spleen	PCa	UK Biobnak	rs85809711	0.015	0.890 (0.864 – 0.917)	4.14e-14	8.54e-04
GGCX	GTEx v8	Stomach	PCa	UK Biobnak	rs85744885	0.025	0.914 (0.871 – 0.959)	2.54e-04	NA
GGCX	GTEx v8	Thyroid	PCa	UK Biobnak	rs85783128	0.025	0.806 (0.768 – 0.846)	3.54e-18	3.08e-03
GGCX	GTEx v8	Skin	PCa	UK Biobnak	rs85788175	0.035	0.753 (0.703 – 0.806)	4.95e-16	1.89e-04
GGCX	GTEx v8	Pancreas	PCa	UK Biobnak	rs85764960	0.044	0.760 (0.698 – 0.829)	4.24e-10	2.26e-01
GGCX	GTEx v8	Esophagus	PCa	UK Biobnak	rs85788175	0.041	0.732 (0.675 – 0.793)	1.81e-14	2.91e-03
GGCX	GTEx v8	Testis	PCa	UK Biobnak	rs85769711	0.021	0.811 (0.777 – 0.846)	1.32e-22	1.10e-04
GGCX	GTEx v8	Adipose	PCa	FinnGen	rs85788175	0.057	0.784 (0.701 – 0.877)	1.98e-05	4.53e-01
GGCX	GTEx v8	Artery	PCa	FinnGen	rs85762048	0.031	0.863 (0.812 – 0.917)	2.16e-06	4.48e-01
GGCX	GTEx v8	Brain	PCa	FinnGen	rs85764041	0.017	0.926 (0.897 – 0.957)	4.54e-06	8.46e-01
GGCX	GTEx v8	Blood vessel_fibroblasts	PCa	FinnGen	rs85758015	0.073	0.767 (0.666 – 0.885)	2.70e-04	1.75e-01
GGCX	GTEx v8	Blood vessel_lymphocytes	PCa	FinnGen	rs85783128	0.017	0.927 (0.898 – 0.958)	6.24e-06	5.71e-01
GGCX	GTEx v8	Colon	PCa	FinnGen	rs85764041	0.041	0.833 (0.769 – 0.903)	8.67e-06	3.85e-01
GGCX	GTEx v8	Heart	PCa	FinnGen	rs85796101	0.038	0.846 (0.785 – 0.912)	1.31e-05	9.91e-01
GGCX	GTEx v8	Muscle	PCa	FinnGen	rs85769711	0.038	0.837 (0.776 – 0.902)	3.56e-06	8.83e-01
GGCX	GTEx v8	Nerve	PCa	FinnGen	rs85788175	0.038	0.843 (0.784 – 0.908)	5.51e-06	3.00e-01
GGCX	GTEx v8	Spleen	PCa	FinnGen	rs85809711	0.021	0.918 (0.881 – 0.956)	3.90e-05	2.75e-01
GGCX	GTEx v8	Stomach	PCa	FinnGen	rs85744885	0.046	0.907 (0.830 – 0.992)	3.22e-02	NA
GGCX	GTEx v8	Thyroid	PCa	FinnGen	rs85783128	0.036	0.843 (0.785 – 0.905)	2.21e-06	5.17e-01
GGCX	GTEx v8	Skin	PCa	FinnGen	rs85788175	0.048	0.808 (0.735 – 0.888)	1.04e-05	4.61e-01
GGCX	GTEx v8	Pancreas	PCa	FinnGen	rs85764960	0.051	0.809 (0.732 – 0.895)	3.62e-05	4.35e-01
GGCX	GTEx v8	Esophagus	PCa	FinnGen	rs85788175	0.054	0.791 (0.711 – 0.879)	1.48e-05	4.28e-01
GGCX	GTEx v8	Testis	PCa	FinnGen	rs85769711	0.034	0.846 (0.791 – 0.905)	9.60e-07	3.03e-01

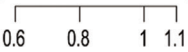


Figure 3. Forest plot illustrating the results of SMR analysis for *GGCX* and prostate cancer (PCa) across multiple tissue types
Abbreviations: HEIDI: Heterogeneity in Dependent Instruments; NA: Not available; OR: Odds ratio; QTL: Quantitative trait loci; SMR: Summary-data-based Mendelian randomization.

epithelial cells, monocytes/macrophages, endothelial cells, and fibroblasts (Figure 5N). Together, these findings indicate that *GGCX* is expressed across several stromal and immune compartments but is most prominently associated with tumor and epithelial cells in the prostate tumor microenvironment, supporting the notion that *GGCX* primarily reflects a tumor cell-intrinsic signal rather than a purely microenvironmental marker.

3.6. Potential pathways linking GGCX to PCa

We first performed differential gene expression analysis using the limma package to characterize genes associated with *GGCX* expression (Figure 6A). This analysis revealed numerous differentially expressed genes, particularly a large set of upregulated genes that might be functionally linked to *GGCX*. We then applied WGCNA to the PCa samples (Figure S1). In this network, the trait representing the top 25% (Q1) of *GGCX* expression showed a significant positive correlation with the turquoise module (r = 0.47, p=6 × 10^{-28}), whereas the trait representing the lowest 25% (Q4) of *GGCX* expression was strongly negatively correlated with this module (r = −0.66, p=6 × 10^{-61}) (Figures 6B, S2A, and S2B). Within the turquoise module, we identified 2,014 genes as potential module members that may be co-regulated with *GGCX*, participate in related biological processes, or act within shared pathways.

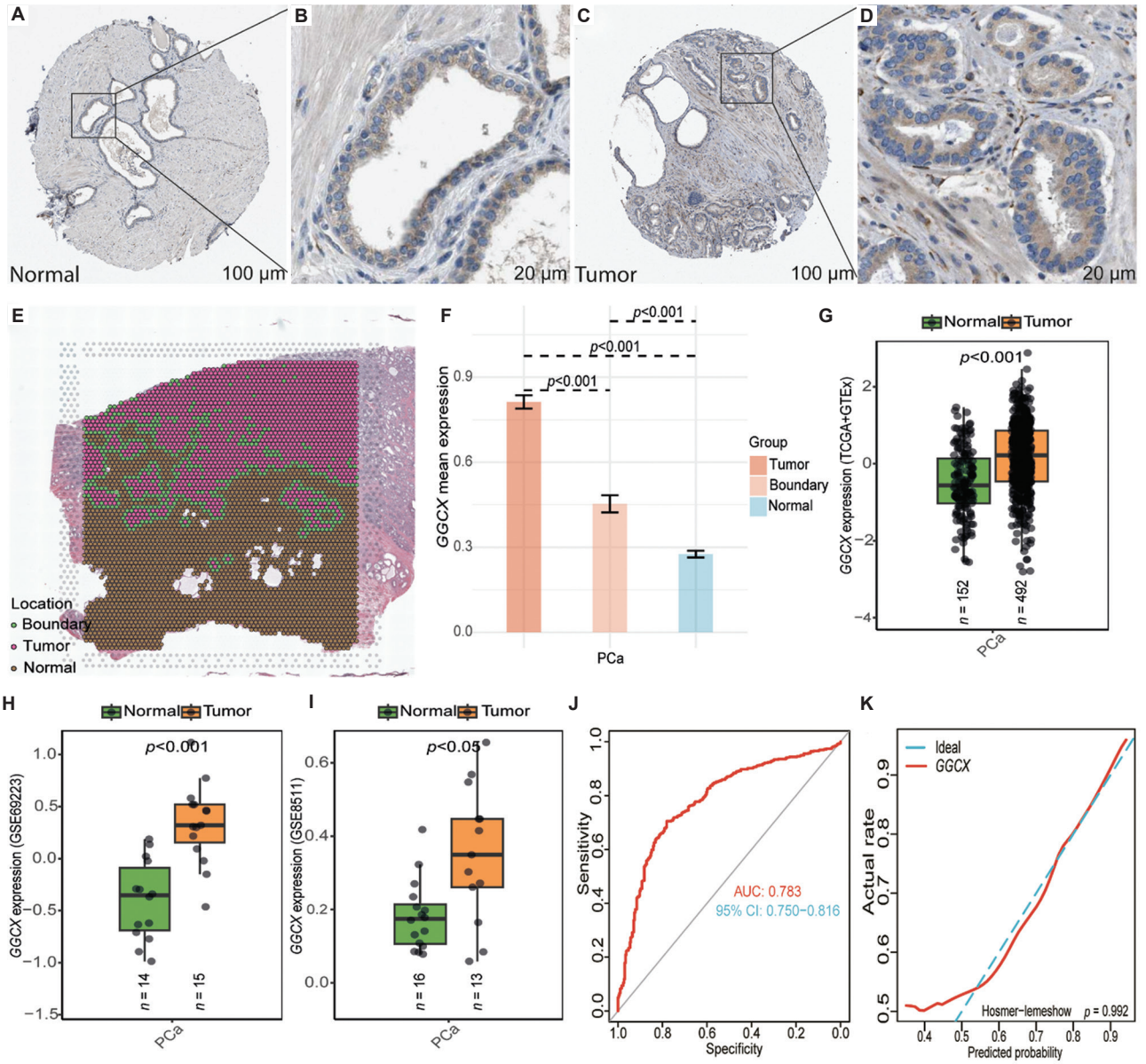


Figure 4. Expression analysis of *GGCX* in prostate cancer (PCa). (A–D) Immunohistochemical staining of *GGCX* in (A and B) normal prostate tissue and (C and D) PCa (scale bars: [A and C] 100 μm and [B and D] 20 μm; magnifications: [A and C] ×100, [B and D] ×400). (E) Spatial transcriptomics analysis illustrating the distribution of malignant, boundary, and normal cells in PCa tissues. (F) *GGCX* expression levels in malignant, boundary, and normal cells within PCa tissue as determined by spatial transcriptomics. (G-I) Differential expression analysis of *GGCX* transcriptional levels in PCa across various datasets. Statistical significance was assessed using the Wilcoxon rank sum test. (J) Receiver Operating Characteristic curve analysis of *GGCX* expression using The Cancer Genome Atlas (TCGA) and normal tissue data from the Genotype-Tissue Expression (GTEx) project. The x-axis represents the specificity, while the y-axis shows the sensitivity. (K) Calibration curve and goodness-of-fit test for *GGCX* gene expression. The x-axis represents the predicted probability of tumor presence, while the y-axis shows the actual observed frequency of tumors.
Abbreviation: AUC: Area under the curve.

To explore the functional context of this *GGCX*-associated module, we carried out GO and KEGG enrichment analyses. GO analysis indicated that these genes were enriched in processes related to endoplasmic reticulum-to-Golgi vesicle-mediated transport, Golgi-associated vesicle membranes, and aminoacyl-tRNA ligase activity, suggesting a close link to protein processing and trafficking. Consistently, KEGG analysis highlighted pathways involved in protein processing in the endoplasmic reticulum, ubiquinone and other terpenoid-quinone biosynthesis, and aminoacyl-tRNA biosynthesis (Figure 6D). We next prioritized the top 200 genes

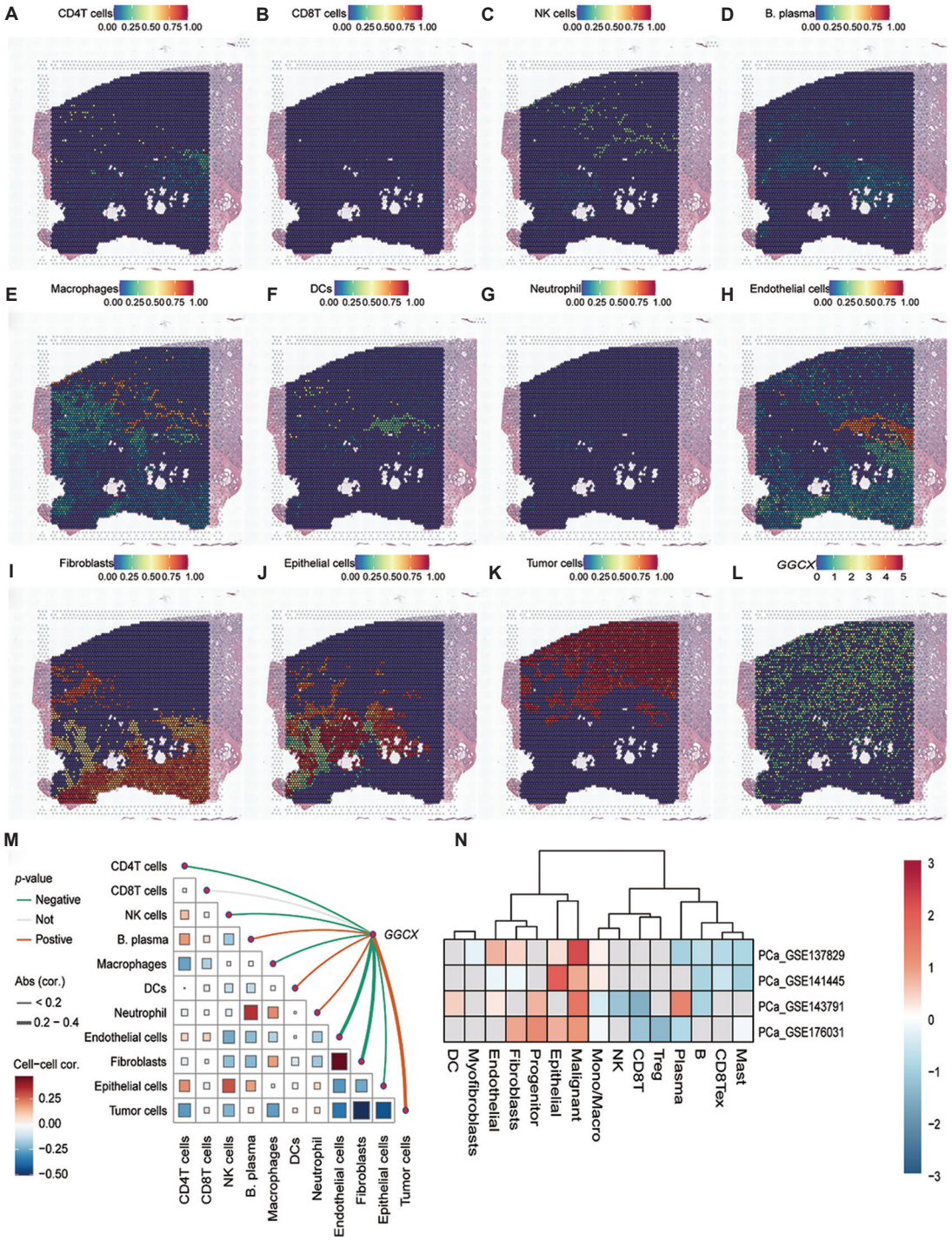


Figure 5. Spatial and transcriptomic analysis of *GGCX* expression in prostate tissue. (A–K) Spatial distribution of all cell types in prostate tissue after deconvolution of spatial transcriptomics data. Each dot represents a spatial transcriptomics spot, with deeper red indicating higher inferred abundance of the indicated cell type in that spot. (L) Spatial mapping of *GGCX* expression. Each dot represents a spatial transcriptomics spot, with deeper red indicating higher levels of *GGCX* expression in that specific spot. (M) Spearman correlation analysis between *GGCX* expression and tumor microenvironment components at spatial resolution. The thickness of the lines corresponds to the absolute value of the correlation coefficient. The triangular correlation heatmap uses color intensity and square size to indicate the strength and significance of the Spearman correlation. (N) Heatmap of *GGCX* expression profiles from the TISCH2 database. Color intensity (red: high expression; grey: no expression/undetected) reflects the expression levels of *GGCX* across various cell types.

Abbreviations: B.: Blood; cor.: Correlation; DC: Dendritic cell; NK: Natural killer; TISCH: Tumor Immune Single-Cell Hub 2; Treg: Regulatory T cell.

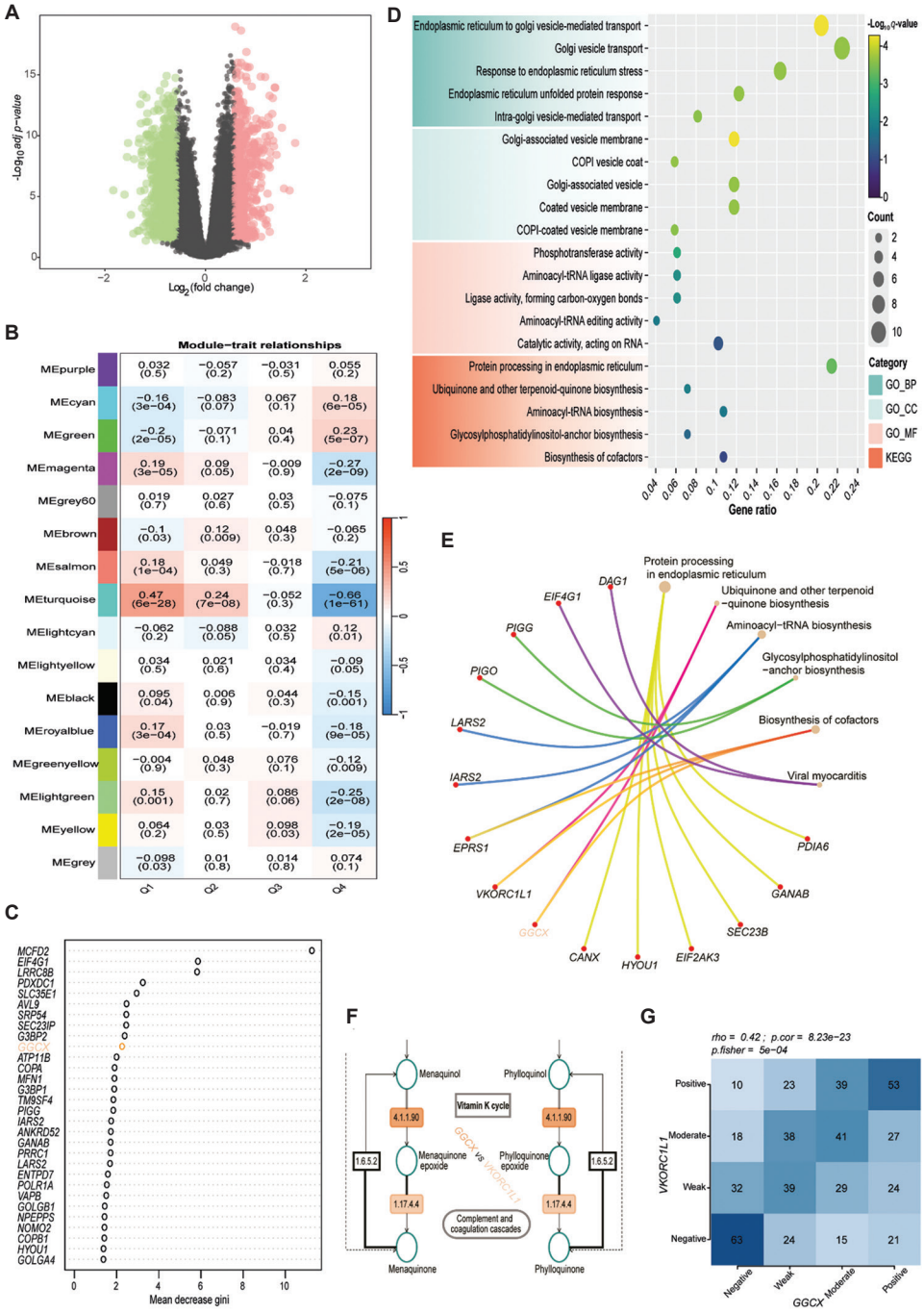


Figure 6. Molecular mechanisms of *GGCX* in prostate cancer (PCa). (A) Volcano plot depicting *GGCX*-associated differentially expressed genes in PCa. (B) Weighted gene co-expression network analysis (WGCNA) showing module–trait relationships. The heatmap highlights the relationships between gene modules and clinical traits, with color intensity representing correlation strength (red: Positive, blue: Negative). Pearson correlation coefficients and associated *p*-values are shown for each module. (C) Feature importance plot from the random forest model. The y-axis lists key features (genes), while the x-axis represents the mean decrease Gini index, quantifying each feature's contribution to model accuracy. Higher values indicate greater importance. (D-F) Functional enrichment analysis visualizing Gene Ontology (GO) and Kyoto Encyclopedia of Genes and Genomes (KEGG) pathways. (D) A bubble plot illustrating GO enrichment analysis, with bubble size representing the proportion of enriched genes within each pathway and color gradient (yellow–green–blue) indicating statistical significance. Pathways are categorized under biological processes (BP), cellular components (CC), and molecular functions (MF). (E) A network plot visualizing the relationships between key genes and enriched pathways identified by KEGG analysis. (F) A partial representation of the ubiquinone and other terpenoid-quinone biosynthesis pathways, with additional details provided in Figure S4. (G) Correlation between *GGCX* and *VKORC1L1*. The analysis includes rho (correlation coefficient), *p*.cor (*p*-value for correlation test), and *p*.fisher (evaluating the independence of gene expression levels).

from this module and compared their expression levels between PCa tumors and normal prostate tissues. This step yielded 51 hub genes that were highly expressed in tumors and significantly associated with *GGCX* expression (Figures S2C and S3, Table S3). To evaluate the relative contribution of *GGCX* within this hub gene set, we built a random forest model and ranked the importance of all 52 candidate genes (51 hubs plus *GGCX*). In this model, *GGCX* consistently ranked within the top 20% of features, indicating that it remains a key contributor within the *GGCX*-related network (Figures 6C, S2E, and S2F).

Finally, we examined the specific pathways that might connect GGCX to PCa biology. We found that *GGCX* and *VKORC1L1* were both enriched in the ubiquinone and other terpenoid-quinone biosynthesis pathway, particularly in components of the vitamin K cycle and complement and coagulation cascades (Figures 6E-G, S2D, and S4). To further validate these findings, we performed GSVA on KEGG metabolic gene sets and compared pathway activity between high- and low-*GGCX* expression groups in the ICGC cohort. The high-*GGCX* group showed activation of several metabolic pathways, with a prominent enrichment of the ubiquinone and other terpenoid-quinone biosynthesis pathway (Figure S5), supporting a role for *GGCX* in vitamin K-related redox and coagulation-associated processes in PCa.

4. Discussion

This multi-omics study identified *GGCX* as a robust susceptibility gene for PCa by integrating cross-tissue SMR, Bayesian colocalization, and large-scale transcriptomic analyses. Across the UK Biobank and FinnGen datasets, genetically predicted *GGCX* expression from blood, whole blood, and prostate groups consistently associated with reduced PCa risk, and *GGCX* was the only gene showing stable colocalization with PCa signals in all tissue-cohort combinations. These convergent genetic findings indicate that germline regulation of *GGCX* contributes to PCa susceptibility through shared cross-tissue regulatory mechanisms rather than a prostate-restricted effect, supporting a potential causal role for *GGCX* in disease initiation. The observation that *GGCX* is also overexpressed in tumors relative to normal prostate tissue in TCGA, GTEx, GEO, and spatial transcriptomic datasets further underscores its central position at the interface between inherited risk and tumor biology.

By combining spatial transcriptomics with cell-type deconvolution, we demonstrated that *GGCX* expression is detectable in multiple stromal and immune compartments and is most prominently enriched in tumor and epithelial cells within the prostate tumor microenvironment. This cell type-resolved view suggests that *GGCX* predominantly reflects a tumor cell-intrinsic program that is nevertheless shaped by, and interacts with, endothelial cells, fibroblasts, and myeloid populations.[34] Such a distribution is consistent with a model in which germline variation in *GGCX* influences the pre-malignant microenvironment—possibly via vascular, stromal, or immune cells—while, once malignancy is established, tumor cells upregulate *GGCX* as part of an adaptive response to local selective pressures.[35,36] The identification of tissue-specific instruments in blood and prostate (for example, rs35215812 and rs6743030) further implies that intervention on *GGCX*-related axes might be designed with some degree of tissue selectivity, potentially limiting off-target effects.

Mechanistically, our network and pathway analyses converge on the vitamin K cycle and associated protein-processing pathways as a plausible axis linking *GGCX* to PCa. Long-term use of vitamin K antagonists, such as warfarin, has been associated with a reduced risk of cancer, particularly PCa.[37-39] The G allele at the rs11676382 locus in *GGCX* has been linked to reduced warfarin dose requirements, with each G allele potentially decreasing warfarin dosage by approximately 6.1%.[40] *GGCX*, together with *VKORC1*/*VKORC1L1*, forms the core of the vitamin K-dependent γ-carboxylation system,[41] which activates Gla-containing proteins involved in coagulation, extracellular matrix organization, vascular calcification, and other aspects of tissue homeostasis.[42,43] Warfarin, by inhibiting *VKORC1*/*VKORC1L1* and blocking KH2 regeneration,[44,45] may indirectly suppress GGCX activity. The enrichment of GGCX-associated modules in endoplasmic reticulum–Golgi vesicle transport, protein processing in the endoplasmic reticulum, ubiquinone and other terpenoid–quinone biosynthesis, and complement and coagulation cascades, together with the positive correlation between *GGCX* and *VKORC1L1* expression, supports a model in which *GGCX* modulates PCa biology through vitamin K-dependent redox and coagulation-related processes.[46,47] Emerging data further indicate that non-canonical vitamin K pathways and *GGCX*-related γ-carboxylation can regulate ferroptosis and oxidative stress, both of which are increasingly recognized as important in PCa progression and therapy response.[47,48] Coupled with epidemiologic and experimental evidence that perturbing vitamin K metabolism can influence cancer risk and behavior, these findings position the GGCX–vitamin K axis as a biologically coherent and potentially druggable pathway in PCa.[49]

At first glance, the protective direction of the SMR estimates (OR < 1) appears to conflict with the consistent overexpression of *GGCX* in tumor tissue. However, this pattern is in line with prior Mendelian randomization work showing that modest, lifelong increases in gene expression

in non-malignant tissues can reduce cancer risk, whereas the same genes may be secondarily upregulated and co-opted by established tumors.[50,51] In our setting, SMR captures the effect of germline variants on baseline *GGCX* expression—potentially in stromal, vascular, or immune compartments—where slightly higher activity may help maintain vascular integrity, the extracellular matrix, and redox balance, and appropriate coagulation–complement signaling, thereby raising the threshold for malignant transformation. By contrast, once oncogenic transformation has occurred, tumor and epithelial cells may increase their reliance on *GGCX* and downstream vitamin K/ubiquinone pathways to cope with heightened protein-folding stress and microenvironmental challenges, resulting in the observed overexpression.[52] This stage- and compartment-dependent behavior implies that *GGCX* is better conceptualized as a context-specific regulator rather than a purely oncogenic or tumor-suppressive gene, with important implications for how and when the GGCX–vitamin K axis might be therapeutically targeted.[46,48]

Several limitations of this work should be carefully considered. First, all genetic and transcriptomic analyses are observational and depend on the core assumptions of summary-based Mendelian randomization and SMR, including the validity of the instruments, linearity, and the absence of horizontal pleiotropy. Residual confounding by linkage disequilibrium, context-specific eQTL effects, or unmeasured biological pathways cannot be fully excluded. The eQTL resources used—derived mainly from non-malignant tissues and predominantly European-ancestry populations—may not fully capture regulatory architectures in other ancestries or in advanced, treatment-exposed tumors. Second, our expression, network, and pathway inferences were based on bulk RNA-seq, deconvolution, and computational modeling, all of which are sensitive to tumor purity, cell-composition shifts, and model assumptions. Although spatial transcriptomics provides important localization information, sample numbers remain limited, and the functional roles of GGCX in specific epithelial, stromal, and immune subsets still require direct perturbation using *in vitro* and *in vivo* models. Finally, the translational implications of targeting the GGCX–vitamin K axis must be approached cautiously, given the systemic impact of vitamin K modulation on coagulation, the potential for confounding in epidemiologic data, and the likelihood that *GGCX* exerts stage- and compartment-dependent effects. Rigorous pre-clinical studies and carefully designed early-phase trials with appropriate pharmacodynamic and safety readouts will be essential before any intervention based on this pathway can be considered for clinical application.

5. Conclusion

The GGCX–vitamin K axis underlies PCa susceptibility, as integrative cross-tissue SMR, colocalization, and transcriptomic analyses link inherited regulation of *GGCX* to a reproducible tumor-associated γ-carboxylation signature. These findings nominate the GGCX–vitamin K axis as a biologically coherent and potentially druggable pathway in PCa, warranting prioritized mechanistic and interventional studies.

Acknowledgments

We would like to express our gratitude to all the participants who contributed to the formation of the GWAS data used in our SMR analysis. We acknowledge the technical support and the R package "grswsci/GroundWork" provided by Dr. Yuyao Liu's research team (https://grswsci.top/). We also thank Mr. Jianmin Xie's team for their visualization platform (https://www.chiplot.online/) and the tools provided by Home for Researchers (https://www.home-for-researchers.com).

Funding

This study was funded by the National Natural Science Foundation of China under grant numbers 82160145 and 82460154, as well as the 2021 National Natural Science Foundation Post Subsidy Individual Fund of China, reference GPPH-NSFC-2021-10. Furthermore, it received support from the Science and Technology Fund of the Guizhou Health Commission, grant number gzwkj2021-212.

Conflict of interest

The authors declare that they have no competing interests.

Author contributions

Conceptualization: Shuxiong Xu, Hua Shi, Yuangao Xu
Formal analysis: Jieyu Xiong, Yuanbo Xu, Yikun Wu, Yuangao Xu
Investigation: Yuangao Xu, Yuanlin Wang
Methodology: Yuangao Xu, Jieyu Xiong, Yuanbo Xu
Writing–original draft: Yuangao Xu, Jieyu Xiong
Writing–review & editing: Shuxiong Xu, Hua Shi

Ethics approval and consent to participate

Not applicable.

Consent for publication

Not applicable.

Availability of data

The GWAS summary statistics, TCGA, ICGC, and GEO datasets utilized in this study are accessible to

authorized investigators through standardized data access procedures.

References

1. Siegel RL, Giaquinto AN, Jemal A. Cancer statistics, 2024. *CA Cancer J Clin*. 2024;74(1):12-49.

   doi: 10.3322/caac.21820

2. Bray F, Ferlay J, Soerjomataram I, Siegel RL, Torre LA, Jemal A. Global cancer statistics 2018: GLOBOCAN estimates of incidence and mortality worldwide for 36 cancers in 185 countries. *CA Cancer J Clin*. 2018;68(6):394-424.

   doi: 10.3322/caac.21492

3. Wilt TJ, Ullman KE, Linskens EJ, *et al*. Therapies for clinically localized prostate cancer: A comparative effectiveness review. *J Urol*. 2021;205(4):967-976.

   doi: 10.1097/ju.0000000000001578

4. Cornford P, Van Den Bergh RCN, Briers E, *et al*. EAU-EANM-ESTRO-ESUR-ISUP-SIOG guidelines on prostate cancer-2024 update. Part I: Screening, diagnosis, and local treatment with curative intent. *Eur Urol*. 2024;86(2):148-163.

   doi: 10.1016/j.eururo.2024.03.027

5. Henriquez I, Spratt D, Gómez-Iturriaga A, Abuchaibe O, Couñago F. Nonmetastatic castration-resistant prostate cancer: Novel agents to treat a lethal disease. *World J Clin Oncol*. 2021;12(1):6-12.

   doi: 10.5306/wjco.v12.i1.6

6. Mizuno K, Ku SY, Venkadakrishnan VB, *et al*. Intraindividual epigenetic heterogeneity underlying phenotypic subtypes of advanced prostate cancer. *Nat Commun*. 2025;16(1):5543.

   doi: 10.1038/s41467-025-60654-z

7. Ahmad F, Cherukuri MK, Choyke PL. Metabolic reprogramming in prostate cancer. *Br J Cancer*. 2021;125(9):1185-1196.

   doi: 10.1038/s41416-021-01435-5

8. Rawat C, Heemers HV. Alternative splicing in prostate cancer progression and therapeutic resistance. *Oncogene*. 2024;43(22):1655-1668.

   doi: 10.1038/s41388-024-03036-x

9. Loizzo D, Pandolfo SD, Rogers D, *et al*. Novel insights into autophagy and prostate cancer: A comprehensive review. *Int J Mol Sci*. 2022;23(7):3826.

   doi: 10.3390/ijms23073826

10. Van Dessel LF, Van Riet J, Smits M, *et al*. The genomic landscape of metastatic castration-resistant prostate cancers reveals multiple distinct genotypes with potential clinical impact. *Nat Commun*. 2019;10(1):5251.

    doi: 10.1038/s41467-019-13084-7

11. Zheng K, Hai Y, Xi Y, *et al*. Integrative multi-omics analysis unveils stemness-associated molecular subtypes in prostate cancer and pan-cancer: Prognostic and therapeutic significance. *J Transl Med*. 2023;21(1):789.

    doi: 10.1186/s12967-023-04683-6

12. GTEx Consortium. The GTEx consortium atlas of genetic regulatory effects across human tissues. *Science*. 2020;369(6509):1318-1330.

    doi: 10.1126/science.aaz1776

13. Võsa U, Claringbould A, Westra HJ, *et al*. Large-scale cis- and trans-eQTL analyses identify thousands of genetic loci and polygenic scores that regulate blood gene expression. *Nat Genet*. 2021;53(9):1300-1310.

    doi: 10.1038/s41588-021-00913-z

14. Kurki MI, Karjalainen J, Palta P, *et al*. FinnGen provides genetic insights from a well-phenotyped isolated population. *Nature*. 2023;613(7944):508-518.

    doi: 10.1038/s41586-022-05473-8

15. Wang A, Shen J, Rodriguez AA, *et al*. Characterizing prostate cancer risk through multi-ancestry genome-wide discovery of 187 novel risk variants. *Nat Genet*. 2023;55(12):2065-2074.

    doi: 10.1038/s41588-023-01534-4

16. Zhu Z, Zhang F, Hu H, *et al*. Integration of summary data from GWAS and eQTL studies predicts complex trait gene targets. *Nat Genet*. 2016;48(5):481-487.

    doi: 10.1038/ng.3538

17. Wu Y, Zeng J, Zhang F, *et al*. Integrative analysis of omics summary data reveals putative mechanisms underlying complex traits. *Nat Commun*. 2018;9(1):918.

    doi: 10.1038/s41467-018-03371-0

18. Giambartolomei C, Vukcevic D, Schadt EE, *et al*. Bayesian test for colocalisation between pairs of genetic association studies using summary statistics. *PLoS Genet*. 2014;10(5):e1004383.

    doi: 10.1371/journal.pgen.1004383

19. Battle A, Brown CD, Engelhardt BE, *et al*. Genetic effects on gene expression across human tissues. *Nature*. 2017;550(7675):204-213.

    doi: 10.1038/nature24277

20. Ding R, Zou X, Qin Y, *et al*. xQTLbiolinks: A comprehensive and scalable tool for integrative analysis of molecular QTLs. *Brief Bioinform*. 2023;25(1):bbad440.

    doi: 10.1093/bib/bbad440

21. Goldman MJ, Craft B, Hastie M, *et al*. Visualizing and interpreting cancer genomics data via the Xena platform. *Nat Biotechnol*. 2020;38(6):675-678.

    doi: 10.1038/s41587-020-0546-8

22. Shi J, Wei X, Xun Z, *et al*. The web-based portal spatialTME integrates histological images with single-cell and spatial transcriptomics to explore the tumor microenvironment. *Cancer Res*. 2024;84(8):1210-1220.

doi: 10.1158/0008-5472.Can-23-2650

23. Pujana-Vaquerizo M, Bozal-Basterra L, Carracedo A. Metabolic adaptations in prostate cancer. *Br J Cancer*. 2024;131(8):1250-1262.

doi: 10.1038/s41416-024-02762-z

24. Xun Z, Ding X, Zhang Y, *et al*. Reconstruction of the tumor spatial microenvironment along the malignant-boundary-nonmalignant axis. *Nat Commun*. 2023;14(1):933.

doi: 10.1038/s41467-023-36560-7

25. Crowell PD, Giafaglione JM, Jones AE, *et al*. MYC is a regulator of androgen receptor inhibition-induced metabolic requirements in prostate cancer. *Cell Rep*. 2023;42(10):113221.

doi: 10.1016/j.celrep.2023.113221

26. Han Y, Wang Y, Dong X, *et al*. TISCH2: Expanded datasets and new tools for single-cell transcriptome analyses of the tumor microenvironment. *Nucleic Acids Res*. 2023;51(D1):D1425-D1431.

doi: 10.1093/nar/gkac959

27. Langfelder P, Horvath S. WGCNA: An R package for weighted correlation network analysis. *BMC Bioinformatics*. 2008;9:559.

doi: 10.1186/1471-2105-9-559

28. The Gene Ontology Consortium. The gene ontology resource: 20 years and still GOing strong. *Nucleic Acids Res*. 2019;47(D1):D330-D338.

doi: 10.1093/nar/gky1055

29. Kanehisa M, Goto S. KEGG: Kyoto encyclopedia of genes and genomes. *Nucleic Acids Res*. 2000;28(1):27-30.

doi: 10.1093/nar/28.1.27

30. Xu S, Hu E, Cai Y, *et al*. Using clusterProfiler to characterize multiomics data. *Nat Protoc*. 2024;19(11):3292-3320.

doi: 10.1038/s41596-024-01020-z

31. Luo W, Brouwer C. Pathview: An R/bioconductor package for pathway-based data integration and visualization. *Bioinformatics*. 2013;29(14):1830-1831.

doi: 10.1093/bioinformatics/btt285

32. Zhang J, Bajari R, Andric D, *et al*. The international cancer genome consortium data portal. *Nat Biotechnol*. 2019;37(4):367-369.

doi: 10.1038/s41587-019-0055-9

33. Wu L, Wang J, Cai Q, *et al*. Identification of novel susceptibility loci and genes for prostate cancer risk: A transcriptome-wide association study in over 140,000 European descendants. *Cancer Res*. 2019;79(13):3192-3204.

doi: 10.1158/0008-5472.Can-18-3536

34. Sabit H, Arneth B, Abdel-Ghany S, *et al*. Beyond cancer cells: How the tumor microenvironment drives cancer progression. *Cells*. 2024;13(19):1666.

doi: 10.3390/cells13191666

35. Zhang R, Qi F, Shao S, Li G, Feng Y. Human colorectal cancer-derived carcinoma associated fibroblasts promote CD44-mediated adhesion of colorectal cancer cells to endothelial cells by secretion of HGF. *Cancer Cell Int*. 2019;19:192.

doi: 10.1186/s12935-019-0914-y

36. Monteran L, Erez N. The dark side of fibroblasts: Cancer-associated fibroblasts as mediators of immunosuppression in the tumor microenvironment. *Front Immunol*. 2019;10:1835.

doi: 10.3389/fimmu.2019.01835

37. Pengo V, Noventa F, Denas G, *et al*. Long-term use of vitamin K antagonists and incidence of cancer: A population-based study. *Blood*. 2011;117(5):1707-1709.

doi: 10.1182/blood-2010-08-304758

38. Dasari S, Ali SM, Zheng G, *et al*. Vitamin K and its analogs: Potential avenues for prostate cancer management. *Oncotarget*. 2017;8(34):57782-57799.

doi: 10.18632/oncotarget.17997

39. Kristensen KB, Jensen PH, Skriver C, Friis S, Pottegård A. Use of vitamin K antagonists and risk of prostate cancer: Meta-analysis and nationwide case-control study. *Int J Cancer*. 2019;144(7):1522-1529.

doi: 10.1002/ijc.31886

40. King CR, Deych E, Milligan P, *et al*. Gamma-glutamyl carboxylase and its influence on warfarin dose. *Thromb Haemost*. 2010;104(4):750-754.

doi: 10.1160/th09-11-0763

41. Shearer MJ, Okano T. Key pathways and regulators of vitamin K function and intermediary metabolism. *Ann Rev Nutr*. 2018;38(1):127-151.

doi: 10.1146/annurev-nutr-082117-051741

42. Hao Z, Jin DY, Chen X, Schurgers LJ, Stafford DW, Tie JK. γ-Glutamyl carboxylase mutations differentially affect the biological function of vitamin K-dependent proteins. *Blood*. 2021;137(4):533-543.

doi: 10.1182/blood.2020006329

43. Berkner KL, Runge KW. Vitamin K-dependent protein activation: Normal gamma-glutamyl carboxylation and disruption in disease. *Int J Mol Sci*. 2022;23(10):5759.

doi: 10.3390/ijms23105759

44. Tie JK, Stafford DW. Structural and functional insights into enzymes of the vitamin K cycle. *J Thromb Haemost*. 2016;14(2):236-247.

doi: 10.1111/jth.13217

45. Li T, Chang CY, Jin DY, Lin PJ, Khvorova A, Stafford DW. Identification of the gene for vitamin K epoxide reductase. *Nature*. 2004;427(6974):541-544.

doi: 10.1038/nature02254

46. Chen A, Li J, Shen N, Huang H, Hang Q. Vitamin K: New insights related to senescence and cancer metastasis. *Biochim Biophys Acta Rev Cancer*. 2024;1879(2):189057.

doi: 10.1016/j.bbcan.2023.189057

47. Ivanova D, Zhelev Z, Getsov P, *et al*. Vitamin K: Redox-modulation, prevention of mitochondrial dysfunction and anticancer effect. *Redox Biol*. 2018;16:352-358.

doi: 10.1016/j.redox.2018.03.013

48. Mishima E, Ito J, Wu Z, *et al*. A non-canonical vitamin K cycle is a potent ferroptosis suppressor. *Nature*. 2022;608(7924):778-783.

doi: 10.1038/s41586-022-05022-3

49. Vinjamuri S, Dontaraju VS, Munirathinam G. Prostate cancer and applications of vitamin K. In: Patel VB, editor. *Molecular Nutrition*. Ch. 29. United States: Academic Press; 2020. p. 613-629.

doi: 10.1016/B978-0-12-811907-5.00027-0

50. Markozannes G, Kanellopoulou A, Dimopoulou O, *et al*. Systematic review of Mendelian randomization studies on risk of cancer. *BMC Med*. 2022;20(1):41.

doi: 10.1186/s12916-022-02246-y

51. Lim YW, Chen-Harris H, Mayba O, *et al*. Germline genetic polymorphisms influence tumor gene expression and immune cell infiltration. *Proc Natl Acad Sci*. 2018;115(50):E11701-E11710.

doi: 10.1073/pnas.1804506115

52. Liu Y, Gusev A, Kraft P. Germline cancer gene expression quantitative trait loci are associated with local and global tumor mutations. *Cancer Res*. 2023;83(8):1191-1202.

doi: 10.1158/0008-5472.Can-22-2624